Materials Horizons

ROYAL SOCIETY OF CHEMISTRY

COMMUNICATION

View Article Online
View Journal | View Issue

Cite this: *Mater. Horiz.*, 2021, 8, 2032

Received 4th April 2021,
Accepted 7th May 2021

DOI: 10.1039/d1mh00556a

rsc.li/materials-horizons

A dual responsive photonic liquid for independent modulation of color brightness and hue†

Yun Liu, [ac] Qingsong Fan,[c] Guanghao Zhu,[b] Gongpu Shi,[a] Huiru Ma,*[b] Wei Li,[a] Tianlong Wu, [a] Jitao Chen,[a] Yadong Yin *[c] and Jianguo Guan *[a]

Responsive chromic materials are highly desirable in the fields of displays, anti-counterfeiting, and camouflage, but their advanced applications are usually limited by the unrealized delicate and independent tunability of their three intrinsic attributes of color. This work achieves the separate, continuous, and reversible modulation of structural color brightness and hue with an aqueous suspension of dual-responsive Fe_3O_4@polyvinylpyrrolidone (PVP)@poly(*N*-isopropyl acrylamide) (PNIPAM) flexible photonic nanochains. The underlying modulation mechanism of color brightness was experimentally and numerically deciphered by analyzing the morphological responses to stimuli. When an increasing magnetic field was applied, the random worm-like flexible photonic nanochains gradually orientated along the field direction, due to the dominant magnetic dipole interaction over the thermal motion, lengthening the orientation segment length up to the whole of the nanochains. Consequently, the suspension displays increased color brightness (characterized by diffraction intensity). Meanwhile, the color hue (characterized by diffraction frequency) could be controlled by temperature, due to the volume changes of the interparticle PNIPAM. The achieved diverse color modulation advances the next-generation responsive chromic materials and enriches the basic understanding of the color tuning mechanisms. With versatile and facile color tunability and shape patterning, the developed responsive chromic liquid promises to have attractive potential in full-color displays and in adaptive camouflages.

New concepts

The developed responsive chromic materials mainly carry out on–off switch or overall changes in color when stimulated by single or multiple stimuli. Limited by the current color modulation methods, the independent delicate modulation of the three intrinsic attributes of color remains a challenge. We demonstrate a structural color brightness modulation principle that relies on the dynamic controllability of the periodic range of the photonic crystalline structures while keeping their lattice constant the same, in order to achieve tunable structural colors with changeable brightness and maintained hue in an aqueous suspension of Fe_3O_4@polyvinylpyrrolidone (PVP)@poly(*N*-isopropyl acrylamide) (PNIPAM) flexible photonic nanochains, by changing the external magnetic field (*H*). The flexible photonic nanochains with random worm-like conformations exhibit gradually increasing periodic ranges along the field direction with increasing field strength, due to the dominant magnetic dipole interaction over the thermal motion. Macroscopically, the suspension displays a continuous and rapid response of color brightness to the strength of *H*. Furthermore, the color hue can be adaptively tuned by altering the temperature when needed. The achievement of a versatile and respective tunability of the color brightness and hue by modulating different external stimuli creates an exciting new avenue for the development of advanced responsive chromic materials.

Introduction

Color plays an essential role in carrying and covering visual information.[1–3] In nature, some living creatures, such as chameleons, turtle beetles, seahorses, and certain fish, can utilize their body color changes for communication of information, temperature regulation, warning or as camouflage, boosting their adaptability to the surrounding environment and survival ability from predators.[4–6] Inspired by these phenomena, a large number of responsive chromic materials that change color in response to external fields such as light, electric field, magnetic field, temperature, pressure, and chemical agents, have been developed for the growing demands within self-adaptive camouflages, intelligent textiles, sensing, smart displays, energy-saving building materials and in fascinating decorations over the past decades.[7–20] However, most of the materials can only carry out the general control of color, especially as an on–off switch or in

[a] *State Key Laboratory of Advanced Technology for Materials Synthesis and Processing, International School of Materials Science and Engineering, Wuhan University of Technology, Wuhan 430070, China. E-mail: guanjg@whut.edu.cn*
[b] *Department of Chemistry, School of Chemistry, Chemical Engineering and Life Science, Wuhan University of Technology, Wuhan 430070, China. E-mail: mahr@whut.edu.cn*
[c] *Department of Chemistry, University of California, Riverside, CA, 92521, USA. E-mail: yadong.yin@ucr.edu*

† Electronic supplementary information (ESI) available: Experimental procedures and additional data. See DOI: 10.1039/d1mh00556a

broad frequency ranges.[7–9,15] In order to meet the critical requirements for their application in full-color displays, high-security anti-counterfeiting and environmentally adaptive camouflage, developing next-generation responsive chromic materials that can adaptively modulate their color hue, saturation, and brightness (HSB) in a respective, continuous, and reversible manner by two or multiple independent external stimuli, is essential.[4,21] So far, such responsive chromic materials are not available, due to the limitations of the existing color modulation mechanisms or the basic materials. Herein, we report a versatile color-changing aqueous liquid that can independently, continuously, and reversibly tune the color brightness and hue by modulating the external magnetic field (H) and surrounding temperature (T), based on the dual responsive individual photonic nanochains (PNCs) of thermosensitive polymer encapsulating superparamagnetic colloidal nanocrystal clusters (CNCs).

While colors generally stem from chemical colorants, brilliant structural colors can be generated through light-matter interactions such as diffraction, scattering, and interference.[22–24] These are environmentally friendly, energy-saving, and anti-photobleaching, demonstrating their increasing importance for future color materials.[25,26] As typical materials exhibiting structural colors, photonic crystals (PCs) are periodically arranged dielectric materials. The photonic band gaps are in the range of the visible spectra when the lattice constants are comparable to the wavelength of visible light.[27] In this case, their diffraction wavelength, diffraction intensity, and peak width at half height correspond to the hue, brightness, and saturation, respectively. When stimuli-responsive materials are used as building blocks or are incorporated into the PCs as the surrounding matrix, the band gaps may be tuned by changing the lattice constant, refractive index, or orientation state, endowing them with dynamic tunability of the structural colors in response to external stimuli, such as pH, T, humidity, electric field and H.[28–34] Among the materials, magnetically responsive PCs have the advantages of having a simple assembly process, being reversible and having a rapid response to H, as well as bright structural colors.[31,35–37] They are based on establishing a balance between the magnetic attraction and the electrostatic or steric repulsion, thus they display tunable color hues that cover the entire visible spectra.[38–40] The one-dimensional periodically arrayed structures of superparamagnetic CNCs can be fixed by inorganic materials or polymers, obtaining various forms of one-dimensional magnetic PCs including films,[41] balls,[30,42–44] fibers,[45] and individual PNCs.[46–50] They can display either constant structural colors or tunable colors with overall changes in HSB when stimulated by a single external field.

In this paper, the independent, continuous, and reversible modulation of structural colors for their brightness and hue has been demonstrated using an aqueous suspension of magnetically and thermally responsive Fe_3O_4@polyvinylpyrrolidone (PVP)@poly(*N*-isopropyl acrylamide) (PNIPAM) flexible PNCs. As indicated by both the experimental and numerical simulation results, the continuous and reversible tunability of the color brightness at a constant color hue benefits from the flexibility of encapsulated PNIPAM and the large chain length, and this guarantees the gradual domination of magnetic interaction over thermal motion with increasing H and enables the orientation and stretch of the chains along the field direction. Consequently, the flexible PNCs exhibit better periodic structures along the field direction under stronger H, leading to enhanced color brightness. Meanwhile, the versatile controllability of the color hue was achieved due to the thermally responsive property of the linking PNIPAM, which adjusts the interparticle distance by volume changes with T. The realization of the diverse tunability of structural color in both brightness and hue can be expected to help develop next-generation chromic materials and enrich the basic understanding of structural color modulation mechanisms. The obtained dual responsive liquid shows great potential for smart structural color materials.

Results and discussion

A dual-responsive aqueous dispersion of Fe_3O_4@polyvinylpyrrolidone (PVP)@poly(*N*-isopropyl acrylamide) (PNIPAM) flexible photonic nanochains (PNCs) was used to investigate the independent, continuous, and reversible modulation of color brightness and hue. The monodisperse Fe_3O_4@PVP colloid nanocrystal clusters (CNCs) with an average diameter of 140 nm (Fig. S1, ESI†) were used as building blocks for the Fe_3O_4@PVP@PNIPAM flexible PNCs, which were fabricated using a hydrogen bond-guided template polymerization method.[49] As shown in Fig. 1a, the formation procedures of the Fe_3O_4@PVP@PNIPAM flexible PNCs include the self-assembly of Fe_3O_4@PVP CNCs induced by external H, and the subsequent *in situ* polymerization of NIPAM initiated by UV light. In the reaction system, PAA functions as a bridge between PVP and NIPAM by forming hydrogen bonds.[49] The formation procedure can be illustrated as follows: first, PAA forms hydrogen bonds with PVP and NIPAM, leading to a much higher NIPAM concentration within the PVP brush shells of Fe_3O_4@PVP CNCs than that outside in the solution. Then, the CNCs with NIPAM within the PVP shells aligned along H with a nearly equal interparticle distance when an external field H was applied. Finally, the polymerization of NIPAM on the Fe_3O_4 particle surface and the interparticle regions was initiated by UV light, resulting in individual one-dimensional periodical nanochains linked by polymers. The addition and amount of PAA significantly influenced the formation of the flexible PNCs, because it determines the amount of NIPAM that is adsorbed onto the surface of the Fe_3O_4@PVP CNCs. The product obtained without the addition of PAA (Fig. S2a, ESI†) exhibits a monodisperse sphere morphology with a rough surface, and this shows no obvious difference compared to the initial Fe_3O_4@PVP CNCs (Fig. S1, ESI†), indicating the poor interaction between PVP and NIPAM. When the PAA concentration was 0.31 mg mL^{-1}, nanochains with a perfect chain structure could still not be obtained due to the insufficient surface coating of PNIPAM (Fig. S2b, ESI†). When the PAA concentration was further increased to 1.67 mg mL^{-1}, flexible PNCs

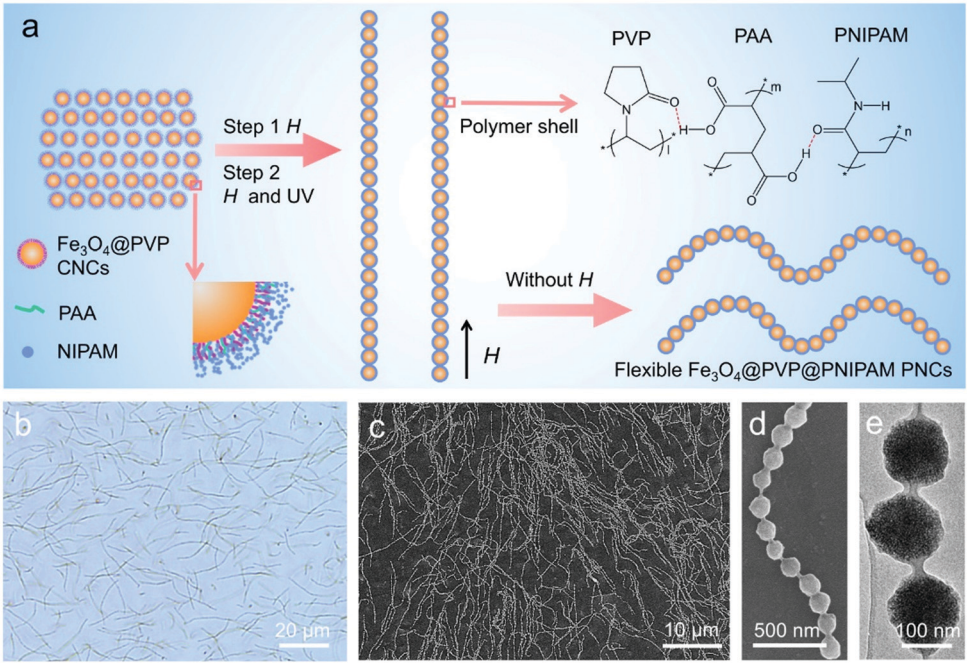

Fig. 1 The preparation and characterization of the typical Fe_3O_4@PVP@PNIPAM flexible PNCs. (a) Schematic illustration showing the formation process of the Fe_3O_4@PVP@PNIPAM flexible PNCs; (b) bright-field optical microscopy image; (c and d) SEM images; (e) TEM image.

could be obtained, but they tended to form bundle chains with thick polymer shells (Fig. S2c, ESI†). The slightly decreased interparticle distance within the nanochains that was obtained at a high PAA concentration was caused by the compression of the PVP brush shells, due to their strong interaction with PAA.

The bright-field optical microscopy image and scanning electron microscopy (SEM) images (Fig. 1b and c, and Fig. S3a in the ESI†) clearly show that the products of the individual nanochains exhibit a randomly natural bending state with an average end-to-end distance (D) of about 13 μm. When an external magnetic field (H) was applied, the nanochains aligned along the field direction with an average chain length (L) of up to about 15 μm, which is larger than D (Fig. S3b and c in the ESI†). This confirms the polymer-analogous flexibility of the nanochains. The magnified SEM image (Fig. 1d), TEM image (Fig. 1e), and the FT-IR spectrum (Fig. S4a, ESI†) reveal that the nanochains are pearl necklace-like structures, in which the particle cores are coated and separated by a PNIPAM layer. The exact mass percentage of polymers was calculated as 34.37%, based on the TG-DSC data (Fig. S4b, ESI†). Furthermore, the superparamagnetic property of the obtained Fe_3O_4@PVP@PNIPAM flexible PNCs, endowing them with the reversible magnetically responsive property, was confirmed by the magnetic hysteresis loop (Fig. S4c, ESI†), which showed negligible remanent magnetization (M_r) and coercivity (H_c) with a mass saturation magnetization (M_s) value of 33.09 emu·g^{-1}.

The aqueous suspension of the obtained Fe_3O_4@PVP@PNIPAM flexible PNCs exhibits independent, continuous, and reversible tunability of diffraction intensity and diffraction wavelength under different H and temperature (T) values. As seen in Fig. 2a, the aqueous suspension of the typical Fe_3O_4@PVP@PNIPAM flexible PNCs at 6 °C exhibited a yellow color, but had enhanced brightness with increasing H. At H = 10 Gs, only a dark yellow color appeared. When H was increased to 50 Gs, a homogeneous color could be observed. The color became much brighter when H was further enhanced to 100 and 400 Gs. The 2D contour map of the reflection spectra (Fig. 2b) confirms that the flexible PNCs under different H values show the same diffraction peak at around 600 nm, but the reflectance (R) increases with the increase in H, and this is consistent with the dark-field optical microscopy observations. This completely distinguishes it from that of the rigid straight magnetic counterparts, of which the structural color brightness is almost independent of the strength of H. According to Bragg's law:

$$\lambda = 2nd \sin\theta, \quad (1)$$

where λ is the diffraction wavelength, n is the relative refractive index, d is the lattice spacing, and θ is the angle between the incident light and the line perpendicular to the axes of the PNCs,[51] the maintained diffraction peaks benefit from the unchanged interparticle distance under a constant temperature. The slight blue shift of the diffraction peak at 10 Gs may be explained by the fact that an external field H of 10 Gs is too low to obtain well-ordered oriented segments within the flexible chains, so the value of θ deviates from 90°. When T was set to 30 °C, the flexible PNCs also showed the same changing trend of color brightness with H, but the diffraction peak was blue shifted to green (560 nm) compared with the case at 6 °C (Fig. 2c and d). Movie S1 (ESI†) shows the dynamic changes of color brightness with H. It can be observed that the color brightness rapidly enhanced as H increased from 0 to 400 Gs, and this then synchronously faded as H decreased from 400 to 0 Gs, indicating that the tuning of the color brightness was a continuous,

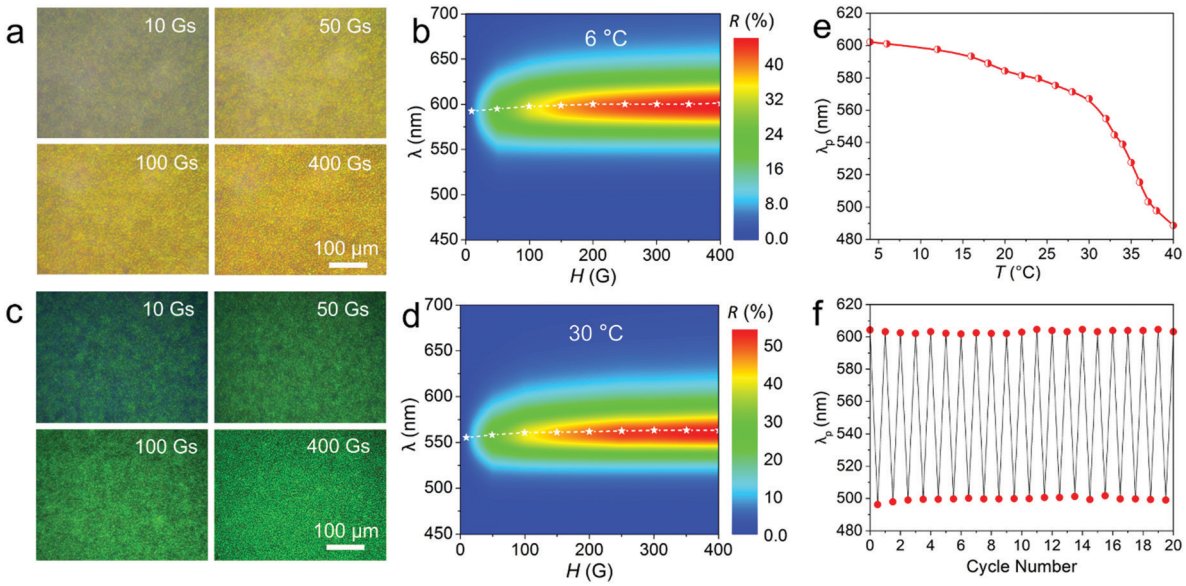

Fig. 2 The dual responsive optical properties of the typical Fe_3O_4@PVP@PNIPAM flexible PNCs. (a and c) Dark-field optical microscopy images, and (b and d) 2D contour maps of the reflection spectra obtained under different *H* and *T* values. (a and b) 6 °C; (c and d) 30 °C. (e) Diffraction wavelength as a function of *T*. (f) Cycling performance showing the variation in diffraction peaks between 4 and 38 °C over 20 cycles. The magnetic field direction in (a and c) is parallel to the observation direction.

reversible, and rapid process. When *T* was further increased to 37 °C, the flexible PNCs still demonstrated increased brightness with an increase in *H*, but the diffraction color further shifted to blue (Fig. S5, ESI†). This suggests a universal phenomenon for the typical flexible PNCs to exhibit magnetic field strength-dependent diffraction intensity.

The dynamic changes of color hue with *T* are shown in Movies S2 and S3 (ESI†). When the sample was stimulated by a drop of ice water (4 °C), the diffraction color changed from green to yellow (Movie S2, ESI†). When it was stimulated by a drop of warm water at 40 °C, the diffraction color rapidly changed from green to blue and then recovered to green (Movie S3, ESI†), showing the reversible tunability of the color hue. The shift in diffraction color was attributed to the thermo-sensitive property of PNIPAM, as this exhibits a reversible transition between the hydrophilic state and the hydrophobic state as *T* changes.[52] When stimulated by warm water, the PNIPAM in the interlayer and in the shell of the nanochains experienced rapid shrinking by expelling water out, leading to a decrease in the interparticle distance and thus a blue shift in the diffraction color. When *T* was recovered to room temperature, PNIPAM returned to a swollen state, leading to increased interparticle distance and the corresponding recovery of the structural color. The as-obtained flexible PNCs showed a more rapid speed of color change than the corresponding thermochromic films and balls,[44,53] and this can be illustrated by their reduced volume change relaxation time:[54]

$$\tau = A^2\pi^{-2}S^{-1}, \quad (2)$$

where *A* is the characteristic length and *S* is the corresponding diffusion coefficient. For the flexible PNCs with a tens-of-nanometers-thick peapod-like PNIPAM shell, *A* could be effectively reduced, ensuring their rapid thermoresponsive property. As shown in Fig. 2e, the diffraction peak (λ_p) blue-shifts from 602 to 489 nm as *T* increases from 4 to 40 °C. The diffraction peak exhibits a rapid decrease at around 32 °C, corresponding to the lower critical solution temperature (LCST) of PNIPAM. Furthermore, the thermoresponsive property is reversible and shows good recycling performance (Fig. 2f). The above results indicate that the obtained aqueous suspension of Fe_3O_4@PVP@PNIPAM flexible PNCs achieves modulation of structural color in both brightness and hue in an independent, continuous, and reversible manner, and this essentially diversifies and enriches the tunability of the structural color. The advantages of versatile shape patterning and adaptive color tuning of the obtained structural color liquid endow it with great potential for applications in full-color displays, in sensors, and in camouflage.

In order to understand the magnetic field strength-dependent optical properties of the flexible PNCs, we recorded *R versus* the magnetic field induction time (*t*) at different *H* values. As shown in Fig. 3a, with an increase of *t*, *R* quickly increases before reaching a constant maximum value (R_{max}). Increasing *H* enhances R_{max} but reduces the shortest time needed for the corresponding R_{max} (t_{min}). The value of t_{min} is almost on the second scale if *H* is stronger than 10 Gs and is typically less than 1 s at a *H* value stronger than 100 Gs. This confirms the swift response of the PNCs to *H*. As depicted in Fig. 3b, the correlation of t_{min} and R_{max} with *H* can be well fitted by the Boltzmann function model, implying that the incorporation of magnetic energy balances the thermal motion of the flexible PNCs, leading to the improvement of R_{max}. The diffraction intensity tunability of the flexible PNCs with *H* may benefit from their polymer-like flexibility and superparamagnetic property, enabling

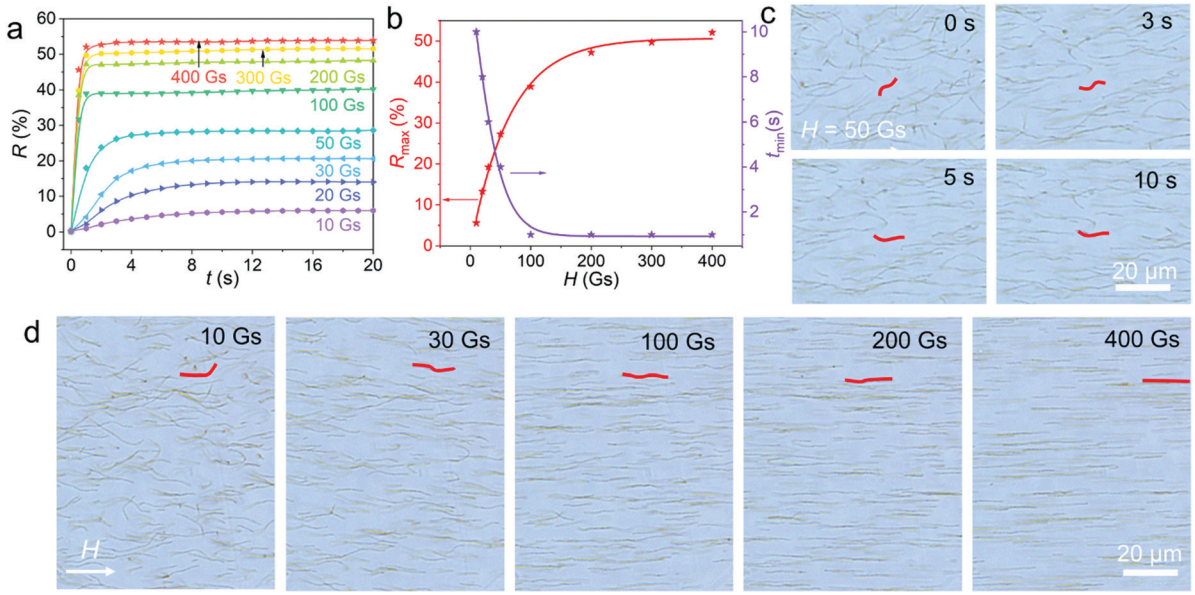

Fig. 3 The influence of H and t on the reflectance and orientation of the typical Fe_3O_4@PVP@PNIPAM flexible PNCs. (a) R, as a function of t at different H values. (b) The influence of H on the corresponding maximum reflectance (R_{max}) and the shortest time needed for R_{max} (t_{min}). The solid lines are the fitted results of the R_{max} and t_{min} data as a function of H based on the Boltzmann model. (c) Bright-field optical microscopy images obtained under 50 Gs with different t values. (d) Bright-field optical microscopy images obtained at different H values with t = 10 s. Typical nanochains are highlighted in red in (c) and in (d) to ease observation.

them to become ordered structures segment by segment with increasing H.

To intuitively substantiate the above assumption, we used optical microscopy to directly observe the orientation process of the flexible PNCs. As shown in Fig. 3c and in Movie S4 (ESI†), when a weak H value of 50 Gs was applied, the randomly dispersed flexible PNCs partly orientated along the field direction as t was increased from 0 to 5 s, but they still exhibited bent segments that could not be stretched into a straight state. When t was extended to 10 s, the PNCs did not show any clear changes in conformation, except for small fluctuations, indicating that the complete stretch orientation could not be achieved at low H by prolonging t, in accordance with the optical property results (Fig. 3a). Fig. 3d shows the balance conformations of the flexible PNCs under different H values. Most of the PNCs did not achieve the deflection orientation along H under 10 Gs. When H was increased to 20 and 30 Gs, the flexible PNCs started to orientate along H, but they existed in an obvious bending state, indicating that the energy supplied by the weak magnetic field was insufficient to balance the thermal motion of most segments and stretch the bent chains. When H was further enhanced to 100 and 200 Gs, most of the flexible long PNCs carried out stretch orientation with a few bent segments. All the PNCs were stretched entirely into a straight state at H = 400 Gs. The small movement towards the field direction under strong H is caused by the magnetic packing force induced by the inhomogeneous magnetic field supplied by a magnet during the observation process. Careful observation indicated that short PNCs are easier for facilitating the complete orientation along H than the long ones, suggesting stronger H dependence of the optical properties for the long flexible PNCs than for the short ones. Movies S5 and S6 (ESI†) show the dynamic orientation process of the flexible PNCs under 400 Gs and when varying H from 0 to 400 to 0 Gs, respectively. The movies confirm the rapid orientation under strong H and a continuous, reversible, and controllable orientation transformation with H, resulting in the tunable periodicity and optical properties of the long flexible PNCs with H.

Based on the microscopy observations, we assumed a schematic illustration for the orientation process of the flexible PNC under H (Fig. 4a). Flexible long PNCs exhibit random worm-like conformations due to the large entropic elasticity endowed by the thermal motion of the flexible PNIPAM gels, and this is similar to in the case of flexible polymer chains associated with the rotation of C–C bonds caused by thermal disturbance.[55,56] When an external field H is applied, the superparamagnetic Fe_3O_4 CNCs in the chain acquire an induced dipole moment:

$$\boldsymbol{m} = \frac{4}{3}\pi r_0^3 \mu_0 \chi \boldsymbol{H}, \quad (3)$$

where μ_0 is the vacuum magnetic permeability, and r_0 and χ are the particle radius and volume susceptibility, respectively.[36] Thus, both the dipole–dipole interaction force:

$$\boldsymbol{F}_d = 3m^2(1 - 3\cos^2\alpha)\boldsymbol{r}d^{-4} \quad (4)$$

(α is the angle between the line connecting the two dipoles and the magnetic field direction, $\boldsymbol{r}$ is the unit vector parallel to the line pointing from two adjacent particles, and d is the center-to-center distance of the two adjacent particles) and the dipole-field packing force:

$$\boldsymbol{F}_p = \nabla(\boldsymbol{mH}) \quad (5)$$

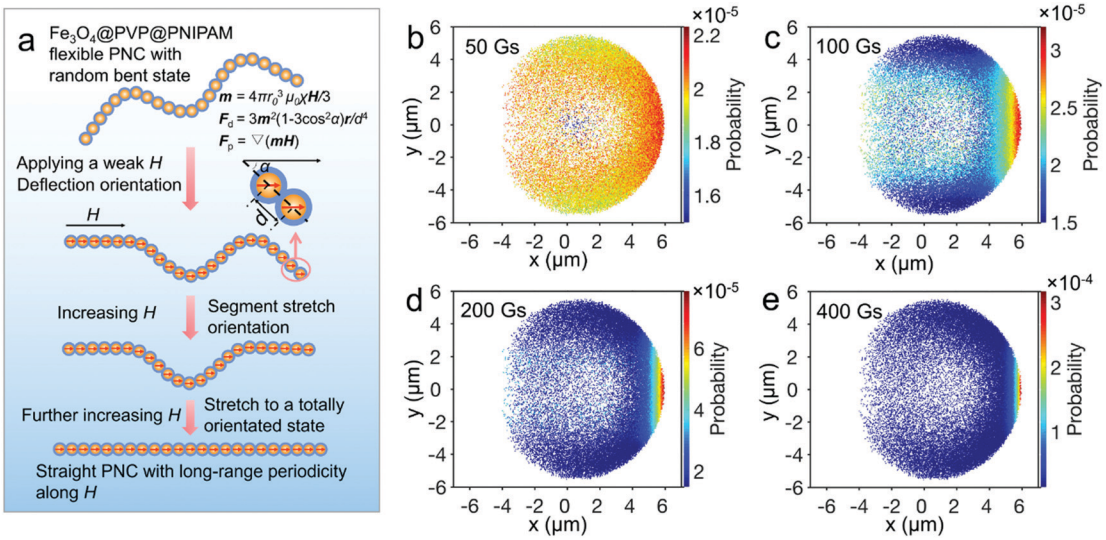

Fig. 4 (a) Schematic illustration for the orientation process of a flexible PNC under H. (b–e) The calculated probabilities of different conformations shown by 50 000 flexible PNCs under different H values.

are induced, in order to minimize the magnetic potential energy.[31,57] When they reach the entropic elasticity of a segment of the flexible PNC, segment stretch orientation occurs along H. The orientated length can be gradually extended by further enhancing H. Thus, all the flexible PNCs could orientate along H when H-induced F_d and F_p are strong enough to balance the entropic elasticity of the whole flexible PNC, ensuring the long-range ordered structure of the entire PNC.

The relationship between the magnetic field strength and the conformation of the flexible PNCs was qualitatively illustrated using a quasi-3D simulation experiment, which gives the probabilities of different chain conformations based on their total energy. The total energy of each flexible PNC at a certain H was calculated by considering the Weeks–Chandler–Andersen (WCA) interaction, the bonding interaction, and the magnetic dipole–dipole interaction.[58,59] With the calculated energy of each conformation, their probabilities were evaluated from the partition functions. A detailed description of the model (Fig. S6, ESI†) and the conformation probability calculation are shown in the ESI.† Fig. S7 (ESI†) shows that most conformations exhibit similar probabilities without H, and this is consistent with the randomly dispersed bending states of the flexible PNCs. The few blue dots in the central area indicate that the probabilities of the corresponding conformations are close to 0, due to the high repulsive WCA potential caused by the overlapping of spheres in those conformations. When a weak magnetic field (50 Gs) is applied along the positive x-direction, the chains with ends at the right side have higher probabilities than those with ends at the top or bottom sides (Fig. 4b). The change in the conformation probabilities with H (Fig. 4b–e) reveals that it becomes more obvious for the PNCs to align themselves along the direction of H to minimize the total energy of the system. When H = 400 Gs, there are much larger probabilities for the PNCs to have ends at the most right-hand side than at the other positions, indicating the most stable conformation of the self-aligned straight state under strong H, and this is consistent with the experimental observations and with the assumption illustrated in Fig. 4a. This reveals that due to the superparamagnetic property of the CNCs, the flexibility of the PNIPAM shells and linkers, and the characteristic large chain length, the flexible PNCs could exhibit balanced states with aligned segments of different lengths along H, showing their unique H-dependent diffraction intensity and color brightness.

As observed from the optical images (Fig. 3d), the smaller the chain lengths, the faster the total orientation occurs along H. Thus, for the flexible PNCs with different average chain lengths (Fig. S8, ESI†), the short PNCs show a more rapid increase in the relative reflectance (R/R_{max}) values with an increase in H than the long ones (Fig. 5a). The higher R/R_{max} values for the short PNCs under weak H can be attributed to their limited disordered segments and rapid total orientation along H, showing the limited tuning ability of the diffraction intensity, and this is consistent with the optical observations. In contrast, long flexible PNCs possess much more disordered segments, which can be stretched to an orientated state gradually by increasing H, guaranteeing their long-range periodic structure under strong H, which is beneficial to obtaining high reflectance and strong brightness. The results further prove that the large chain length is essential for the flexible PNCs to obtain magnetic field strength-dependent tunability for color brightness.

In addition to the large chain length, the magnetic field strength-dependent diffraction intensity of the Fe_3O_4@PVP@PNIPAM flexible PNCs also benefits from their flexibility that originates from the soft property of the linking PNIPAM. The flexible PNCs with different cross-linking degrees were obtained by tuning the molar ratio of BIS and NIPAM (δ) during the preparation procedure (Fig. S9, ESI†). As seen from Fig. S10 (ESI†), the flexible Fe_3O_4@PVP@PNIPAM PNCs with δ = 2%, 5%, and 10% all exhibit a magnetic field tunable diffraction intensity due to the intrinsic soft property of PNIPAM. When H = 0–50 Gs, the PNCs with δ = 10% exhibit larger R/R_{max} values

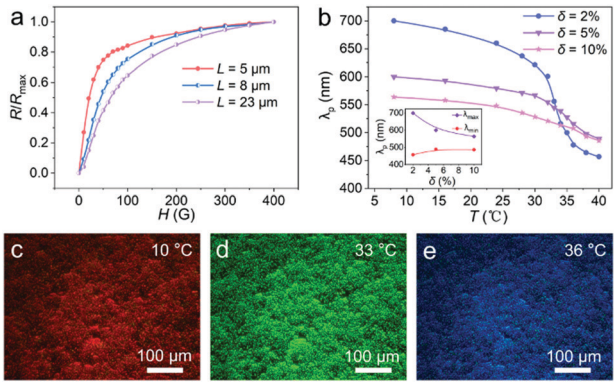

Fig. 5 The influence of L and δ on the optical properties of the Fe_3O_4@PVP@PNIPAM flexible PNCs. (a) Plots showing the magnetic field strength responsive optical properties of the flexible PNCs with different L values. (b) Plots showing the temperature-responsive optical properties of the flexible PNCs with different δ values. The inset in (b) shows the maximum and minimum diffraction wavelengths of the flexible PNCs with different δ values. (c–e) Dark-field optical microscopy images of the flexible PNCs with δ = 2% at different temperatures.

than those with δ = 2% and 5%, which only show negligible differences with irregular fluctuations. When H = 50–400 Gs, the R/R_{max} values of the PNCs at a certain H value increase as δ increases from 2% to 5%, but they decrease as δ further increases from 5% to 10%. The rapid increase of the R/R_{max} values for the PNCs with δ = 10% at weak H can be attributed to their rapid rotation orientation along the field direction, and this benefits from their less bending original conformations. With an increase in H, the orientation of the flexible PNCs is dominated by the segment stretch orientation along H, and the PNCs with lower δ possess more disordered segments, resulting in a slower increase in the R/R_{max} values. However, flexible PNCs with δ = 10% exhibit a decreased sensitivity of magnetic field strength due to their reduced flexibility and the high magnetic energy needed for the stretch of segments with enhanced mechanical strength. The flexible nanochains with different cross-linking degrees at a certain H value slightly differ in their R/R_{max} values from an overall perspective. This phenomenon could be reasonably explained by the full consideration that the PNCs obtained with different δ values have different intrinsic soft attributes of PNIPAM, and different lattice distances and polymer content of PNCs.

While the crosslinking degree of the flexible Fe_3O_4@PVP@PNIPAM PNCs does not significantly influence their magnetic field strength-responsive optical property, their temperature-responsive optical property is clearly affected. Fig. 5b shows that the tuning range of the diffraction wavelength decreases from 243 to 78 nm as δ increases from 2% to 10%. The maximum diffraction wavelength (λ_{max}) for the flexible PNCs of different δ values decreases with increasing δ. In contrast, the minimum diffraction wavelength (λ_{min}) first increases as δ increases from 2% to 5%, and then remains almost constant as δ further increases from 5% to 10%. The higher λ_{max} and lower λ_{min} values for flexible PNCs with δ = 2% indicate their larger and smaller interparticle distance at low and high temperatures. This confirms that the low crosslinked flexible PNCs show strong swelling or shrinking ability due to the loose structure of the polymer networks, guaranteeing their good temperature responsiveness. The flexible PNCs with δ = 2% achieved tunable hues ranging from red to blue (Fig. 5c–e), and their continuous and reversible temperature-responsive color change progress is shown in Movie S7 (ESI†). The results demonstrate that the tunability of the color hue covering the entire visible light spectrum can be achieved by simply adjusting the crosslinking degree of the linking PNIPAM. Furthermore, the Fe_3O_4@PVP@PNIPAM flexible PNCs with original diffraction colors ranging from red to blue could be easily obtained by tuning the reaction parameters during the sample fabrication process (Fig. S11, ESI†), which could be utilized to control the structural parameters of the flexible PNCs and thus their dual-responsive properties. By combining the delicate fabrication process and the respective or combined stimuli of magnetic field and temperature, targeted structural colors with independent, continuous, and reversible modulation in brightness and hue could be achieved by the developed aqueous suspension of Fe_3O_4@PVP@PNIPAM flexible PNCs.

Conclusions

In summary, the independent, continuous, and reversible modulation of structural colors in brightness and hue has been achieved by an aqueous suspension of dual responsive Fe_3O_4@PVP@PNIPAM flexible PNCs. Benefiting from the superparamagnetic property of Fe_3O_4@PVP CNCs, the soft nature of the linking PNIPAM, and the large chain length, the as-obtained flexible PNCs show gradual stretching orientation along the field direction, due to the domination of their magnetic potential energy over their entropic elasticity in an increasing external magnetic field, ensuring the enhancement of diffraction intensity and structural color brightness. The tunability of the structural color brightness of the flexible PNCs relies on their large chain-length and flexibility. Meanwhile, the hue of the flexible PNCs can be easily tuned by changing the surrounding temperature due to the temperature-dependent volume shrinking or swelling behavior of PNIPAM. Furthermore, the delicate fabrication of the flexible PNCs with different original colors and the single or combined stimuli of magnetic field and temperature could be utilized to achieve target colors with predesigned brightness and hue. The independent, continuous, and reversible tunability of structural colors in brightness and hue of the developed photonic liquid promises the next generation of adaptive chromic materials and enriches the basic understanding of color modulation mechanisms.

Author contributions

J. G. and H. M. conceived the idea and designed the experiments. H. M., Y. Y. and J. G. supervised the project. Y. L., G. Z., G. S. and J. C. conducted the experiments and analyzed the results.

Y. L., Q. F., W. L. and T. W. designed and conducted the simulation calculations. Y. L. and Q. F. wrote the manuscript. H. M., Y. Y. and J. G. revised the manuscript. All authors contributed to the discussion and preparation of the manuscript.

Conflicts of interest

There are no conflicts to declare.

Acknowledgements

This work was financially supported by the National Key R&D Program of China (2020YFA0710100), the National Natural Science Foundation of China (51521001), the Natural Science Foundation of Hubei Province (2019CFB572), the Fundamental Research Funds for the Central Universities (WUT: 2017-YB-003), and the China Scholarship Council (CSC). Yin is grateful for the financial support from the US National Science Foundation (DMR-1810485).

References

1 P. Wu, J. Wang and L. Jiang, *Mater. Horiz.*, 2020, **7**, 338–365.
2 C. Fenzl, T. Hirsch and O. S. Wolfbeis, *Angew. Chem., Int. Ed.*, 2014, **53**, 3318–3335.
3 E. S. A. Goerlitzer, R. N. K. Taylor and N. Vogel, *Adv. Mater.*, 2018, **30**, 1706654.
4 L. Shang, W. Zhang, K. Xu and Y. Zhao, *Mater. Horiz.*, 2019, **6**, 945–958.
5 J. Teyssier, S. V. Saenko, D. van der Marel and M. C. Milinkovitch, *Nat. Commun.*, 2015, **6**, 6368.
6 Y. Zhao, Z. Xie, H. Gu, C. Zhu and Z. Gu, *Chem. Soc. Rev.*, 2012, **41**, 3297–3317.
7 A. Abdollahi, H. Roghani-Mamaqani and B. Razavi, *Prog. Polym. Sci.*, 2019, **98**, 101149.
8 A. Abdollahi, H. Roghani-Mamaqani, B. Razavi and M. Salami-Kalajahi, *ACS Nano*, 2020, **14**, 14417–14492.
9 Y. Wang, Q. Zhao and X. Du, *Mater. Horiz.*, 2020, **7**, 1341–1347.
10 T. H. Park, H. Eoh, Y. Jung, G. W. Lee, C. E. Lee, H. S. Kang, J. Lee, K. B. Kim, D. Y. Ryu, S. Yu and C. Park, *Adv. Funct. Mater.*, 2021, **31**, 2008548.
11 S. Li, Y. Zeng, W. Hou, W. Wan, J. Zhang, Y. Wang, X. Du and Z. Gu, *Mater. Horiz.*, 2020, **7**, 2944–2950.
12 Y. Wang, Y. Yu, J. Guo, Z. Zhang, X. Zhang and Y. Zhao, *Adv. Funct. Mater.*, 2020, **30**, 2000151.
13 Y. Yang, Y. Chen, Z. Hou, F. Li, M. Xu, Y. Liu, D. Tian, L. Zhang, J. Xu and J. Zhu, *ACS Nano*, 2020, **14**, 16057–16064.
14 S. U. Kim, S. H. Lee, I. H. Lee, B. Y. Lee, J. H. Na and S. D. Lee, *Opt. Express*, 2018, **26**, 13561.
15 A. C. Arsenault, D. P. Puzzoo, I. Manners and G. A. Ozin, *Nat. Photonics*, 2007, **1**, 468–472.
16 H. Fudouzi and Y. N. Xia, *Langmuir*, 2003, **19**, 9653–9660.
17 J. Hou, M. Li and Y. Song, *Angew. Chem., Int. Ed.*, 2018, **57**, 2544–2553.
18 Y. Cui, Y. Ke, C. Liu, Z. Chen, N. Wang, L. Zhang, Y. Zhou, S. Wang, Y. Gao and Y. Long, *Joule*, 2018, **2**, 1707–1746.
19 C. Xiong, J. Zhao, L. Wang, H. Geng, H. Xu and Y. Li, *Mater. Horiz.*, 2017, **4**, 862–868.
20 Z. Li, J. Jin, F. Yang, N. Song and Y. Yin, *Nat. Commun.*, 2020, **11**, 1–11.
21 Y. Bao, Y. Yu, H. Xu, C. Guo, J. Li, S. Sun, Z. Zhou, C. Qiu and X. Wang, *Light: Sci. Appl.*, 2019, **8**, 95.
22 B. M. Boyle, T. A. French, R. M. Pearson, B. G. McCarthy and G. M. Miyake, *ACS Nano*, 2017, **11**, 3052–3058.
23 J. Hou, M. Li and Y. Song, *Nano Today*, 2018, **22**, 132–144.
24 J. Chen, J. Feng, Z. Li, P. Xu, X. Wang, W. Yin, M. Wang, X. Ge and Y. Yin, *Nano Lett.*, 2019, **19**, 400–407.
25 A. G. Dumanlia and T. Savin, *Chem. Soc. Rev.*, 2016, **45**, 6698–6724.
26 Y. Li, Q. Fan, X. Wang, G. Liu, L. Chai, L. Zhou, J. Shao and Y. Yin, *Adv. Funct. Mater.*, 2021, 2010746.
27 E. Yablonovitch, *Phys. Rev. Lett.*, 1987, **58**, 2059–2062.
28 Z. Li and Y. Yin, *Adv. Mater.*, 2019, 1807061.
29 J. Ge and Y. Yin, *Angew. Chem., Int. Ed.*, 2011, **50**, 1492–1522.
30 H. Ma, Y. Tan, J. Cao, S. C. Lian, K. Chen, W. Luo and J. Guan, *J. Mater. Chem. C*, 2018, **6**, 4531–4540.
31 L. He, M. Wang, J. Ge and Y. Yin, *Acc. Chem. Res.*, 2012, **45**, 1431–1440.
32 F. Yang, F. Mou, Y. Jiang, M. Luo, L. Xu, H. Ma and J. Guan, *ACS Nano*, 2018, **12**, 6668–6676.
33 L. Bai, Z. Xie, W. Wang, C. Yuan, Y. Zhao, Z. Mu, Q. Zhong and Z. Gu, *ACS Nano*, 2014, **8**, 11094–11100.
34 X. Jia, T. Zhang, J. Wang, K. Wang, H. Tan, Y. Hu, L. Zhang and J. Zhu, *Langmuir*, 2018, **34**, 3987–3992.
35 M. Wang and Y. Yin, *J. Am. Chem. Soc.*, 2016, **138**, 6315–6323.
36 Z. Li, M. Wang, X. Zhang, D. Wang, W. Xu and Y. Yin, *Nano Lett.*, 2019, **19**, 6673–6680.
37 Z. Li, F. Yang and Y. Yin, *Adv. Funct. Mater.*, 2019, 1903467.
38 W. Luo, H. Ma, F. Mou, M. Zhu, J. Yan and J. Guan, *Adv. Mater.*, 2014, **26**, 1058–1064.
39 H. Wang, Q. Chen, Y. Yu, K. Cheng and Y. Sun, *J. Phys. Chem. C*, 2011, **115**, 11427–11434.
40 J. Ge, L. He, J. Goebl and Y. Yin, *J. Am. Chem. Soc.*, 2009, **131**, 3484–3486.
41 C. Li, X. Zhou, K. Wang, K. Li, M. Li and Y. Song, *Compos. Commun.*, 2019, **12**, 47–53.
42 Y. Zhao, L. Shang, Y. Cheng and Z. Gu, *Acc. Chem. Res.*, 2014, **47**, 3632–3642.
43 J. Ge, H. Lee, L. He, J. Kim, Z. Lu, H. Kim, J. Goebl, S. Kwon and Y. Yin, *J. Am. Chem. Soc.*, 2009, **131**, 15687–15694.
44 W. Luo, J. Yan, Y. Tan, H. Ma and J. Guan, *Nanoscale*, 2017, **9**, 9548–9555.
45 S. Shang, Z. Liu, Q. Zhang, H. Wang and Y. Li, *J. Mater. Chem. A*, 2015, **3**, 11093–11097.
46 H. Wang, Q. Chen, Y. Sun and M. He, *J. Phys. Chem. C*, 2010, **114**, 19660–19666.
47 Y. Hu, L. He and Y. Yin, *Angew. Chem., Int. Ed.*, 2011, **50**, 3747–3750.
48 H. Ma, K. Tang, W. Luo, L. Ma, Q. Cui, W. Li and J. Guan, *Nanoscale*, 2017, **9**, 3105–3113.

49 W. Luo, Q. Cui, K. Fang, K. Chen, H. Ma and J. Guan, *Nano Lett.*, 2020, **20**, 803–811.
50 L. Kong, Y. Feng, W. Luo, F. Mou, K. Ying, Y. Pu, M. You, K. Fang, H. Ma and J. Guan, *Adv. Funct. Mater.*, 2020, 2005243.
51 J. M. Weissman, H. B. Sunkara, A. S. Tse and S. A. Asher, *Science*, 1996, **274**, 959–963.
52 F. Mou, C. Chen, Q. Zhong, Y. Yin, H. Ma and J. Guan, *ACS Appl. Mater. Interfaces*, 2014, **6**, 9897–9903.
53 H. Ma, M. Zhu, W. Luo, W. Li, K. Fang, F. Mou and J. Guan, *J. Mater. Chem. C*, 2015, **3**, 2848–2855.
54 K. Matsubara, M. Watanabe and Y. Takeoka, *Angew. Chem., Int. Ed.*, 2007, **46**, 1688–1692.
55 T. T. Perkins, D. E. Smith and S. Chu, *Science*, 1997, **276**, 2016–2021.
56 D. E. Smith and S. Chu, *Science*, 1998, **281**, 1335–1340.
57 D. Lisjak and A. Mertelj, *Prog. Mater. Sci.*, 2018, **95**, 286–328.
58 J. Wei, F. Song and J. Dobnikar, *Langmuir*, 2016, **32**, 9321–9328.
59 X. Xue and E. P. Furlania, *Phys. Chem. Chem. Phys.*, 2014, **16**, 13306–13317.